Biophysical Reports

ARTICLE

Anisotropic presentation of ligands on cargos modulates degradative function of phagosomes

Mengchi Jiao,[1] Wenqian Li,[1] Yanqi Yu,[1] and Yan Yu[1,*]
[1]Department of Chemistry, Indiana University, Bloomington, Indiana

ABSTRACT Anisotropic arrangement of cell wall components is ubiquitous among bacteria and fungi, but how such functional anisotropy affects interactions between microbes and host immune cells is not known. Here we address this question with regard to phagosome maturation, the process used by host immune cells to degrade internalized microbes. We developed two-faced microparticles as model pathogens that display ligands on only one hemisphere and simultaneously function as fluorogenic sensors for probing biochemical reactions inside phagosomes during degradation. The fluorescent indicator on just one hemisphere gives the particle sensors a moon-like appearance. We show that anisotropic presentation of ligands on particles delays the start of acidification and proteolysis in phagosomes, but does not affect their degradative capacity. Our work suggests that the spatial presentation of ligands on pathogens plays a critical role in modulating the degradation process in phagosomes during host-pathogen interactions.

SIGNIFICANCE There is increasing recognition that bacteria and fungi have anisotropic surfaces. However, there is virtually nothing known about how such microbial surface anisotropy might impact the pathogen-host interactions. By developing Moon particle sensors as model pathogens, here we drew a direct connection between the surface anisotropy of particles and its functional consequences on the degradative activities within phagosomes encapsulating the particles. The discovery that the anisotropic presentation of ligands delays the onset of phagosome degradation suggests a possible mechanism by which pathogens might alter their surface anisotropy to perturb host immune responses.

INTRODUCTION

Surface anisotropy is ubiquitous on microbes, and many bacteria have asymmetric surface structures. Some have bipolar organization, with flagella, pili, and stalks on one pole (1). Bacterial bipolarity can also result from variation in cell wall composition, with dividing bacteria cells being the most notable example (2). The surface anisotropy of bacteria seems to be functionally important. It is known to play an important role in determining how they adhere to solid surfaces (3). It can also impact host-pathogen interactions. The gram-negative bacterium *Bradyrhizobium* was found to preferentially attach to cells of the soybean seed coat by its older pole, where lectin BJ38 was concentrated (4). However, the importance of bacterial surface anisotropy has only been recognized recently owing to the development of advanced imaging techniques (5,6). Very little is yet known about its functional consequences. In particular, little is known about how the anisotropic distribution of surface proteins on pathogenic microorganisms affects their interactions with mammalian immune cells. Such interactions could have serious consequences in the pathogenesis of infectious diseases (7).

Host-pathogen interactions involve two critical processes: phagocytosis and the degradation of pathogens. Phagocytosis is triggered when innate immune receptors recognize pathogen-associated molecular patterns. Detected pathogens are engulfed into intracellular vacuoles called phagosomes. These phagosomes then degrade and destroy their cargo in a maturation process. During maturation, phagosomes undergo a series of biochemical transformations in both membrane composition and lumenal environment, through which they acquire their degradative capacity (8). Specifically, phagosomes remodel their membranes by recruiting

Submitted August 20, 2021, and accepted for publication December 7, 2021.

*Correspondence: yy33@iu.edu

Editor: Erdinc Sezgin.

https://doi.org/10.1016/j.bpr.2021.100041

functional lipids and special membrane proteins (9), generate reactive oxygen species (10), acidify in their lumen (11), and activate proteases for pathogen degradation (12). Previous studies using synthetic particles as model pathogens have revealed that phagocytosis is affected by the physiochemical parameters of the ingested cargos. Particle size (13), shape (14), and mechanical stiffness (15) have all been shown to affect the probability of internalization (also known as phagocytosis efficiency) of particles by phagocytic immune cells. The surface density of ligands also seems to play a role, but results have been contradictory (16,17). The impact of physiochemical properties of particles on phagosome maturation has been much less studied, but the type of ligand on the surface of a particle has been shown to affect the kinetics of maturation (18-20). All those studies were done using synthetic particles with uniform surface coatings of ligands as model pathogens. In our previous study, we fabricated two-faced Janus particles that display ligands on only one hemisphere. Owing to the anisotropic presentation of ligands, those particles were internalized by cells via combined mechanisms of ligand-dependent phagocytosis and ligand-independent macropinocytosis (21,22). However, it remains unclear how the anisotropic distribution of ligands on particles might affect the maturation and degradative function of phagosomes after the internalization step.

In this study, we address this question by directly showing the effect of anisotropic ligand presentation of particles on the degradative function of phagosomes. To do so, we engineered two-faced Janus particle sensors (3 μm) as phagocytic cargos. These particles were designed to not only have anisotropic ligand presentation, but also to enable *in situ* imaging and measurements of the degradative functions of single phagosomes, including lumen acidification and proteolysis, by means of fluorogenic indicators. Because the particle sensors fluoresce from only one hemisphere, their appearance resembles that of the changing phase of the Moon. We, therefore, refer to them as "Moon" particles. With so-called pHMoon and proteolysis-Moon particles, we revealed that the anisotropic distribution of ligands on a particle changes the kinetics of phagosome maturation and degradation. This included altered recruitment of early phagosome markers, delayed acidification and proteolysis, and reduced acidification kinetic rate. It did, however, have a negligible effect on the final degradative capacity of phagosomes. This finding suggests that intracellular pathogens might use their surface anisotropy to delay the onset of phagosome degradation to prolong their survival and to increase infection inside host immune cells.

MATERIALS AND METHODS

Materials

Silica particles of 3 μm in diameter were purchased from Spherotech. Sodium orthovanadate (Na_3VO_4), 4-(2-hydroxyethyl)-1-piperazineethanesulfonic acid (HEPES), pHrodo iFL Red STP Ester, EZ-Link N-hydroxysuccinimide ester biotin (NHS-Biotin), and streptavidin (SAv) were purchased from ThermoFisher Scientific. The 3-aminopropyltriethoxysilane (APTES) was from Acros Organics. Paraformaldehyde (PFA) and dimethyl sulfoxide (DMSO) were from Avantor. CF640R-NHS and CF488-NHS were purchased from Biotium. SYLGARD 184 polydimethylsiloxane (PDMS) kit, albumin from bovine serum (BSA), IgG from rabbit plasma, diphenyleneiodonium chloride, 1,1′-carbonyldiimidazole (CDI), and Amicon Ultra filters (30K) were purchased from MilliporeSigma. Curdlan (β-1,3-glucan from *Alcaligenes faecalis*) was purchased from InvivoGen. Alexa Fluor 488 and Alexa Fluor 647 conjugated phospho-Syk (Tyr525/526) rabbit monoclonal antibody (4349S) was from Cell Signaling Technology. Nigericin sodium salt was purchased from Tocris Bioscience. FuGENE HD transfection reagent was purchased from Promega. RAW 264.7 macrophage cells were obtained from American Type Culture Collection. RAW 264.7 cells stably expressing actin-mCherry or actin-green fluorescent protein (GFP), as well as LAMP1-GFP plasmid, 2×FYVE-GFP plasmid, Rab7-GFP plasmid, and LC3-GFP plasmid were kindly provided by Prof. Sergio Grinstein (University of Toronto, Ontario, Canada). Dectin-1 GFP-expressing RAW 264.7 macrophages were originally provided by Prof. David Underhill at Cedars-Sinai Medical Center. Ringer's solution (pH = 7.2, 10 mM HEPES, 10 mM glucose, 155 mM NaCl, 2 mM NaH_2PO_4, 5 mM KCl, 2 mM $CaCl_2$, 1 mM $MgCl_2$) was used for macrophage live-cell imaging. Ringer's solution adjusted to a pH of 4.5, 5.5, 6.5, and 7.2 was used for extracellular pH calibration of pHMoon Sensors. Potassium-rich buffer (135 mM KCl, 2 mM K_2HPO_4, 1.2 mM $CaCl_2$, 0.8 mM $MgSO_4$) adjusted to a pH of 4.5, 5.5, 6.5, and 7.2 was used for intracellular pH calibration of pHMoon Sensors.

Cell culture, transfection, and pharmacological treatments

All RAW 264.7 cells were cultured in Dulbecco's Modified Eagle Medium (DMEM) complete medium supplemented with 10% fetal bovine serum, 2 mM L-glutamine, 100 U/mL penicillin, and 100 μg/mL streptomycin at 37°C and 5% CO_2. Transfection was carried out according to the manufacturer's instructions. In brief, 0.25 million RAW 264.7 macrophages were seeded on a precleaned 30 mm glass coverslip without antibiotics 24 h before transfection. After replacing the cell medium with complete DMEM medium without antibiotics, 2 μL 500 ng/mL plasmid was then mixed with 3 μL FuGENE HD transfection reagents in 95 μL DMEM medium without supplements for 15 min. The mixture was then gently added to cells. Cells were incubated overnight before use.

Protein labeling

To prepare SAv-pHrodo Red, SAv (concentration in mixture: 1 mg/mL) was mixed with pHrodo Red STP ester (concentration in mixture: 160 μg/mL) in sodium bicarbonate buffer (0.1 M, pH 8.25) and incubated at room temperature for 2 h on rotor. Free dyes were then removed by centrifugation using Amicon 30K filters at 14,000 rcf at 4°C for 10 min. Protein concentration and degree of dye labeling were measured using a Thermofisher NanoDrop Nd-1000 microvolume spectrophotometer. The same procedure was used for preparing SAv-CF640R. Concentration of SAv and CF640R-NHS ester in the

reaction mixture was 1 mg/mL and 120 μg/mL, respectively. To prepare IgG-biotin, IgG (concentration in mixture: 1 mg/mL) was mixed with biotin-NHS (concentration in mixture: 25 μg/mL) and then incubated in bicarbonate buffer (0.1 M, pH 8.25) at room temperature for 2 h on rotor. Free biotin-NHS was then removed by centrifugation using Amicon 50K filter at 14,000 rcf at 4°C for 10 min. IgG-biotin concentration was measured using Nanodrop. The same procedure was used for preparing CF488-IgG-biotin. The concentration of IgG-biotin and CF488-NHS ester in the reaction mixture was 1 mg/mL and 80 μg/mL, respectively.

Fabrication of Moon particle sensors

Gold-coated Janus particles were fabricated following a previously described protocol (21). Briefly, 3-μm silica particles were first etched in piranha solution (3:1 v/v H_2SO_4 to 30% H_2O_2) at 80°C for 15 min and then rinsed with deionized (DI) water. Next, particles were dried in a desiccator for 30 min, resuspended in ethanol, and prepared into monolayers on pre-etched glass microscope slides. The particle monolayer was coated sequentially with chromium (15 nm thick) and gold (30 nm) using an Edwards thermal evaporator (Nanoscale Characterization Facility at Indiana University). The gold-coated particles were sonicated off microscope slides in ethanol. Particles were then centrifuged, washed with ethanol, and resuspended in 1.2 mL 3% v/v APTES ethanol solution. After incubation overnight, particles were centrifuged and washed with ethanol and dried in a desiccator for 30 min.

To fabricate IgG-coated pHMoon Sensors, Janus particles after the APTES conjugation step were incubated with 0.34 mg/mL biotin-NHS in 1 mL sodium bicarbonate buffer (0.1 M, pH 8.25) for 1 h on rotor, followed by washing in phosphate-buffered saline (PBS). Particles were then incubated for 25 min with a PBS solution containing 2% (w/w) BSA. Afterward, SAv-pHrodo Red and SAv-CF640R were added into the mixture at the concentration of 1 μg/mL and 7.5 μg/mL, respectively. After 1 h incubation, particles were washed with PBS and resuspended in PBS solution containing 4 μg/mL IgG-biotin for another 1 h incubation. Particles were then washed in PBS buffer and stored at 4°C hidden from light. Particle concentration in the solution was estimated using a hemocytometer. To fabricate IgG-coated proteolysis-Moon particle sensors, Janus IgG particles with only CF640R-SAv were synthesized in the same protocol as above. The particles were then incubated with 125 μg/mL $(Phe\text{-}Arg)_2$-Rh100 in PBS solution for 1 h. Particles were washed in PBS solution and stored at 4°C hidden from light. To fabricate curdlan-coated pHMoon Sensors, silica Janus particles after the APTES conjugation step were mixed with 0.5 M CDI in anhydrous DMSO and the mixture was vortexed at room temperature for 1 h. Afterward, particles were rinsed and resuspended in DMSO containing 1 mg/mL curdlan. The mixture was vortexed at room temperature for 2 h. Particles were then rinsed with DMSO and PBS, and then incubated for 25 min in PBS solution containing 2% (w/w) BSA. Afterward, SAv-pHrodo Red and SAv-CF640R were added into the mixture at the concentration of 1 μg/mL and 7.5 μg/mL, respectively. Particles were then washed in PBS and stored at 4°C hidden from light.

Moon particles were created using a microcontact printing method (23) in experiments where the spatial distribution of GFP markers on phagosomes was examined to eliminate the possibility that the metal coating on the Moon particles might affect the GFP fluorescence. Briefly, the PDMS substrate was fabricated by mixing a base and a curving agent at a 10:1 ratio to a total mass of 11 g in a Petri dish. Subsequently, bubbles were removed by vacuum and the mixture was baked overnight at 70°C. A 1 cm × 1 cm PDMS was prepared and placed on a clean glass coverslip. A drop of piranha solution (1:1 v/v H_2SO_4 to 30% H_2O_2) was applied on the stamp for 5 min, followed by DI water wash. A drop of 5 mg/mL IgG-CF640R in a PBS solution was applied onto the stamp and incubated for 25 min in darkness. The stamp was then washed with PBS and DI water. After air drying, the stamp was immediately pressed against a monolayer of clean silica particles with a pressure of 1.5×10^4 Pa for 3 min. The stamp was peeled off and placed in a 0.75 mL 50 μg/mL BSA in a PBS solution. Particles were sonicated off, washed with PBS, and harvested by centrifugation.

Live cell microscopy

Epifluorescence images were acquired using a Nikon Eclipse Ti microscope equipped with a Nikon 1.49 N.A. 100× TIRF objective, a Hamamatsu ORCA-Fusion digital CMOS camera, and an Andor iXon3 EMCCD camera. Re-Scan confocal microscopy images were acquired using the RCM module (by Confocal.nl) added on the Nikon Eclipse Ti microscope. For live-cell imaging, 0.5 million RAW 264.7 macrophages were seeded on a pre-etched 30 mm coverslip overnight before experiments. Cells were incubated in a serum-free medium for 2 h and washed with PBS. Particles dispersed in 1 mL of Ringer's solution were added to cells, followed by 30 s spin down at 200 rcf. Live-cell imaging was performed at 37°C.

(1) In single-phagosome acidification rate and final pH measurements, time-lapse multi-channel epifluorescence images were acquired to record the fluorescence emission of pHrodo Red (ex, 562 nm; em, 605 nm) and CF640R dyes (ex:, 640 nm; em, 700 nm). At the end of imaging each sample, cells were washed and incubated in pH 4.5 potassium-rich buffer containing 10 mM nigericin for 10 min for pH calibration. The fluorescence intensity ratio between pHrodo Red and CF640R was converted to pH and then plotted as a function of time. In single-phagosome acidification standby time measurement, pHMoon particle sensors were incubated with RAW 264.7 macrophages stably expressing actin-GFP. The fluorescence emission of actin-GFP (ex, 482 nm; em, 525 nm) was acquired together with pHrodo Red and CF640R using epifluorescecnce microscopy. The time at actin-GFP peak was set to 0 s, as it indicates the completion of phagocytosis (24). In Dectin-1-mediated phagosome acidification experiments, curdlan pHMoon particle sensors were incubated with RAW 264.7 macrophages stably expressing Dectin-1 GFP.
(2) In single-phagosome proteolysis measurements, proteolysis-Moon particle sensors were incubated with RAW 264.7 macrophages stably expressing actin-mCherry. Time-lapse multi-channel epifluorescence images were acquired to record the fluorescence emission of Rhodamine 110 from the peptide (ex, 482 nm; em, 525 nm), CF640R (ex, 640 nm; em, 700 nm), and actin-mCherry (ex, 545 nm; em, 605 nm). The fluorescence intensity of individual proteolysis-Moon Sensors was analyzed using the same protocol for pHMoon particles.
(3) In single phagosome actin remodeling and PI(3)P recruitment experiments, the fluorescence emission of 2×FYVE-GFP or actin-GFP was acquired together with that of CF640R from the particle sensors using epifluorescecnce microscopy. The GFP intensity of the phagosomes was normalized by the local cytosolic GFP background. In GFP intensity vs. time plots, time at GFP intensity peak was set to 0 s.
(4) In Rab7, LAMP1, and LC3 recruitment experiments, particles were incubated with RAW 264.7 macrophages transiently transfected with corresponding GFP-markers for 40 min before imaging.

Calibration of pHMoon Sensors

For extracellular calibration, pHMoon Sensors were added into 1 mL pH 7.2 Ringer's solution in an imaging chamber. The buffer was then

switched sequentially to a pH of 6.5, 5.5, and 4.5 Ringer's solution. At each pH, the fluorescence emission of pHrodo Red and CF640R was acquired using epifluorescecnce microscopy. Intracellular pH calibration of pH sensors was done following a previously published protocol (25,26). RAW 264.7 cells stably expressing actin-GFP were seeded as described above. Cells were then incubated with 10 μM concanamycinA in serum-free DMEM solution for 5 min. The medium was switched to pH 7.2 Ringer's buffer and then pHMoon particles were added to cells. After identifying actin-GFP signal increase, which indicated particle phagocytosis, the Ringer's buffer was then replaced sequentially with a pH of 7.2, 6.5, 5.5, and 4.5 potassium-rich buffers containing 10 mM nigericin. At each pH, cells were rinsed twice in the appropriate buffer and allowed to equilibrate for 10 min before image acquisition. Fluorescence emission of pHrodo Red and reference dye CF640R was obtained at each pH using epifluorescecnce microscopy. Fluorescence intensity of individual pHMoon Sensors was analyzed using single-particle tracking Matlab algorithm (25,27) with some modifications. In live-cell acidification measurements, an internal calibration curve was generated for individual pH sensors based on their $I_{pHrodoRed}/I_{CF640R}$ at pH 7.2 in cell and at pH 4.5 after potassium-rich buffer calibration. This helped to eliminate the potential effect of particle-to-particle variation in pH calibration (25,26). To measure pHMoon intensity as a function of particle orientation, pHMoon Sensors were suspended in a mixture of glycerol and PBS buffer (1:1 v/v). Fluorescence emission of pHrodo Red and reference dye CF640R of single particles at different orientations was obtained using epifluorescecnce microscopy as described above.

In vitro calibration of proteolysis-Moon Sensors

Proteolysis-Moon Sensors were mixed with 1 mg/mL trypsin in pH 7.2 Ringer's solution in 96-well plates. The concentration of particle sensors was estimated using hemocytometer and the number of particle sensors was kept the same in all samples. The fluorescence emission of rhodamine 110 from the peptide (ex, 489 nm; em, 530 nm) was measured for 1 h at 37°C using a Biotek Synergy H1 microplate reader.

Immunofluorescence staining

Cells were seeded as described above. We added 1 mM Na_3VO_4 in the serum-free medium and then cells were incubated with particles for 10 min at 37°C with 5% CO_2. Cell samples were washed with ice-cold PBS solution, fixed with 2% PFA on ice for 5 min, permeabilized with acetone at −20°C for 5 min, blocked with 2% BSA and 22.5 mg/mL glycine at room temperature for 30 min, and then stained with 2 μg/mL Alexa Fluor 488 conjugated phospho-Syk antibody or Alexa Fluor 647 conjugated phospho-Syk antibody at room temperature for 1 h.

Sigmoidal-Boltzmann fitting

The pH-time plots of single phagosomes were fitted with the sigmoidal-Boltzmann equation (28):

$$pH(t) = pH_{final} + \frac{pH_{initial} - pH_{final}}{1 + e^{\frac{t - t_{1/2}}{dt}}},$$

in which t is time, $pH_{initial}$ and pH_{final} are the initial and final pH, respectively, $t_{1/2}$ is the half-response time when pH = 1/2 ($pH_{initial} + pH_{final}$), and dt is a constant. Slope at $t_{1/2}$ is the acidification rate by definition:

$$Acidification\ Rate = \frac{pH_{initial} - pH_{final}}{4dt}.$$

After the phagocytosis point indicated by actin-GFP peak intensity was set to 0 s, the acidification standby time was calculated as:

$$Acidification\ Standby\ Time = t_{1/2} - 2dt$$

The fluorescence intensity of cleaved peptides from single phagosomes also follows a sigmoidal-Boltzmann relationship with time:

$$I(t) = I_{final} + \frac{I_{initial} - I_{final}}{1 + e^{\frac{t - t_0}{dt}}},$$

in which $I(t)$ is the normalized peptide intensity at time t, I_0, and I_t are the initial and final peptide intensity, respectively, $t_{1/2}$ is the half-response time when $I(t) = 1/2\ (I_0 + I_t)$ and dt is a constant. The proteolysis rate and proteolysis standby time were calculated the same way as acidification.

Statistical analysis

The Kruskal-Wallis test with Dunn's test as a *post hoc* test was performed for multiple-group comparisons. Statistical significance is indicated as follows: ****$p < 0.0001$, ***$p < 0.001$, **$p < 0.01$, *$p < 0.05$, and not significant (ns) $p > 0.05$. Statistic figures were plotted using OriginLab Pro 2021.

RESULTS

Fabrication and calibration of pHMoon particles

To measure phagosomal acidification, the pHMoon Sensors were prepared by first coating a thin layer of gold film onto one hemisphere of 3-μm silica particles to create a surface anisotropy, which was confirmed using scanning electron microscopy (Fig. 1 *B*). The non-coated silica hemisphere was biotinylated, conjugated with pHrodo Red-streptavidin (SAv) and CF640R-SAv, and then further functionalized with biotinylated immunoglobulin G (IgG) (Fig. 1 *A*). The entire particles were blocked with BSA. pHrodo Red is a pH indicator that emits intense fluorescence in an acidic environment. Its fluorescence intensity is sensitive to pH within a range that matches the range of pH changes inside phagosomes (29). CF640R was used as a reference dye due to its photostability and pH insensitivity (Fig. S1). The SAv serves as a cushion layer to separate the pHrodo Red dye from the particle surface, as we observed that pHrodo Red becomes insensitive to pH changes when directly conjugated on particles (25). From fluorescence images, we confirmed the anisotropic presentation of SAv and IgG on pHMoon particles (Fig. 1 *C*).

To characterize the response of pHMoon particle sensors, we measured the fluorescence intensity ratio between pHrodo Red and CF640R ($I_{pHrodo\ Red}/I_{CF640R}$) on single particle sensors both in buffer solutions and in cells at different pH levels. Both extracellular (Fig. S2 *A*) and intracellular calibration plots (averaged plots in Fig. 1 *D* and individual plots in Fig. S2 *C*) show that $I_{pHrodoRed}/I_{CF640R}$ increases linearly with pH from

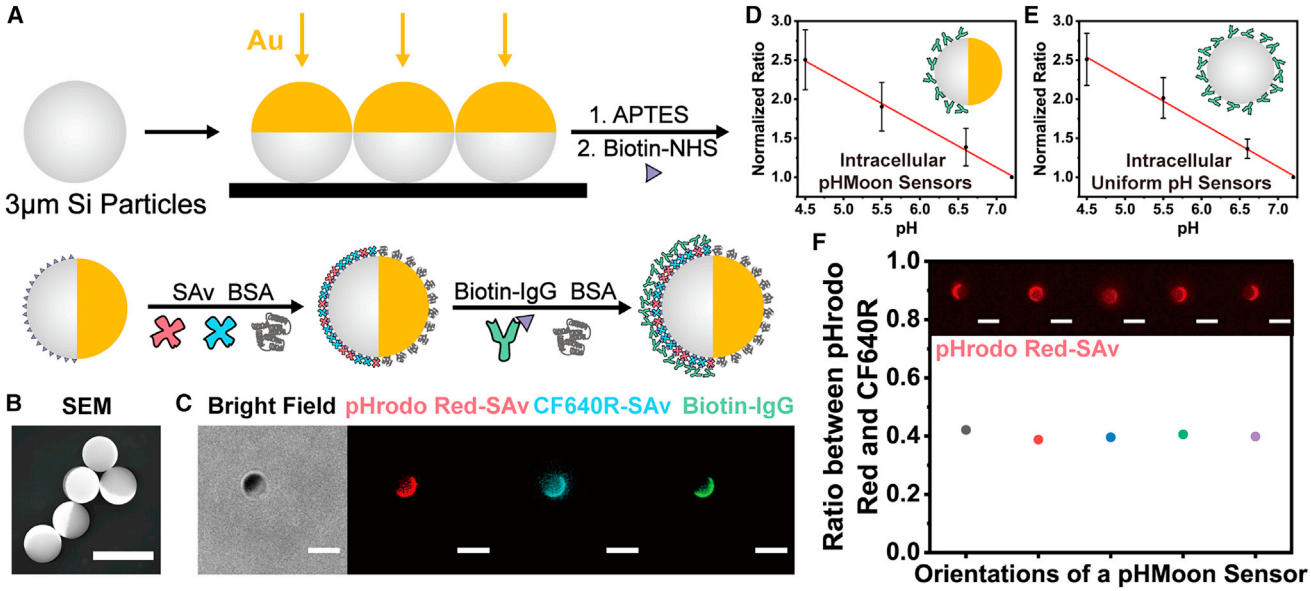

FIGURE 1 Fabrication and characterization of pHMoon Sensors. (*A*) Schematic illustration of the fabrication procedure of pHMoon Sensors. (*B*) Scanning electron microscope image of particles half-coated with gold. (*C*) Bright-field and epifluorescence images of pHMoon Sensors. SAv is the abbreviation for streptavidin. (*D* and *E*) Averaged intracellular calibration of pHMoon Sensors (n = 19, $R^2 = 0.9979$) (*D*) and uniform pH sensors (n = 14, $R^2 = 0.9970$) (*E*). Error bar represents the standard deviation. (*F*) Ratiometric pHrodo Red/CF640R fluorescence of a single pHMoon Sensor at different orientations imaged with epifluorescence microscopy. Scale bars in all images, 5 μm.

7.2 to 4.5, which is the range of pH expected during phagosome maturation (9). To determine whether having pHrodo Red-SAv and CF640R-SAv on only one hemisphere affects the pH response of pHMoon particles, we performed the same pH calibration using particles that were uniformly functionalized with pHrodo Red-SAv, CF640R-SAv, and IgG. These uniform particles exhibited pH responses that were similar to those of pHMoon particles, confirming that the two-faced Janus geometry had no effect on pH measurements (Figs. 1 *E* and S2, *B* and *D*). As the gold coating on one hemisphere of the pHMoon particle sensors can block fluorescence emission from the other hemisphere, we further examined $I_{pHrodoRed}/I_{CF640R}$ of single pHMoon particles as they rotate to different orientations in glycerol. Consistent with what we reported previously, each pHMoon particle appeared like the moon in projection epifluorescence images and its "crescent"-shaped fluorescence profile changed as it rotated (Fig. 1 *F*) (30). The $I_{pHrodoRed}/I_{CF640R}$ of a single particle remained constant at different particle orientations, confirming that the pH response is not affected by particle orientation.

Effect of anisotropic ligand presentation of particles on early phagosome markers and actin remodeling

We sought to investigate how the anisotropic presentation of ligands on particles affects the assembly of phagosomes during phagocytosis. During this process, the binding of fragment crystalizable gamma receptors (FcγR) to IgG on particles drives membrane engulfment. We therefore began by examining the activation of FcγRs by IgG on the particle sensors. We immunostained phosphorylated spleen tyrosine kinase (pSyk) after stimulating cells with Moon particles (without pHrodo Red dyes) for 10 min. Because Syk is recruited to the cytoplasmic domain of activated FcRs and becomes phosphorylated for downstream signaling (31), the presence of pSyk is a direct indicator of FcγR activation. As shown in Fig. 2 *A*, we observed intense immunofluorescence of pSyk on the portion of a phagosome membrane that was in contact with the IgG-coated hemisphere of the Moon particles. The colocalized distribution of pSyk on phagosomes and IgG on particles is further demonstrated by their line-scan intensity distribution along the circumference and across the diameter of phagosomes (Figs. S3–S5). By comparison, pSyk was homogeneously distributed on phagosomes encapsulating particles with a uniform coating of IgG. Particles with only BSA blocking served as a negative control, as they were known to be internalized by a macropinocytosis-like mechanism, not mediated by phagocytic receptors (32). Negligible pSyk labeling was observed on macropinosomes containing particles with a uniform coating of BSA. These results show that FcγRs are activated by IgG on particles and that their distribution on phagosomes follows the spatial presentation of ligands. Because the binding of FcγR to IgG on particles drives membrane

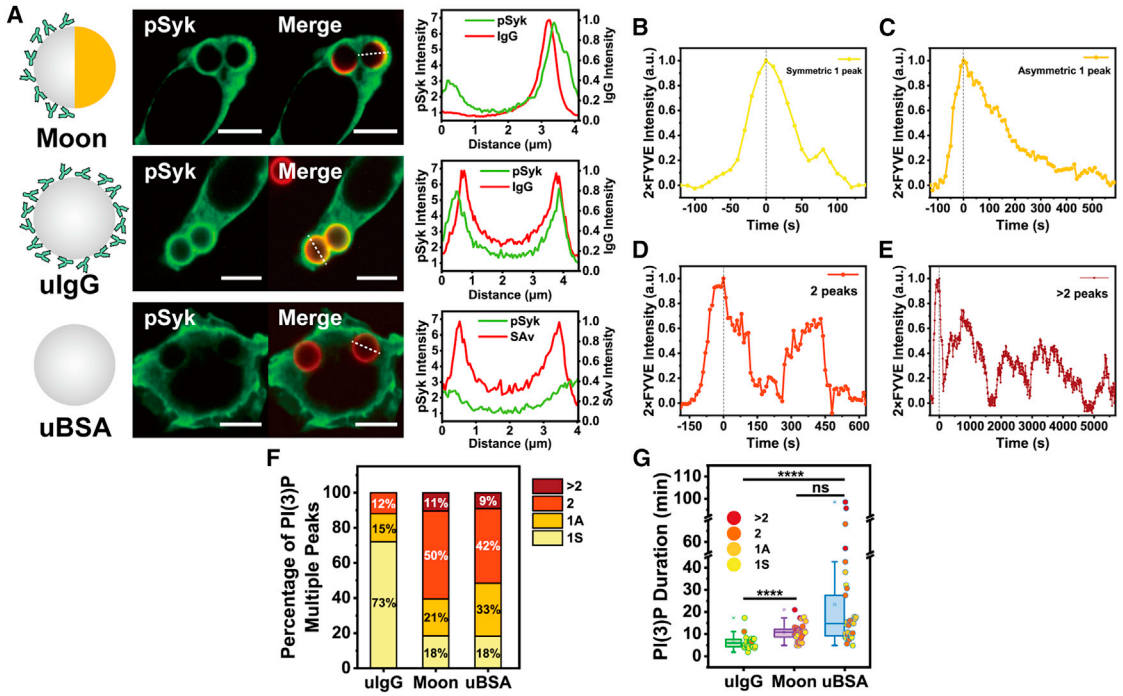

FIGURE 2 Distribution of pSyk and PI(3)P association on phagosomes containing Moon particles. pSyk was immunostained and PI(3)P was marked by 2×FYVE-GFP. (*A*) Rescan confocal microscopy images and line-scan plots showing the pSyk distribution on phagosomes containing Moon particles and uniform IgG (uIgG) particles, and on macropinosomes containing uniform BSA (uBSA) particles. (*B–E*) Representative PI(3)P intensity-time plots showing different kinetics of PI(3)P on phagosomes: Symmetric one peak (*B*), asymmetric one peak (*C*), two peaks (*D*), and multiple (>2) peaks (*E*). The time at 2×FYVE-GFP peak was arbitrarily set as time zero. (*F*) The percentage of phagosomes that exhibited a symmetric single peak (1S), an asymmetric single peak (1A), two peaks (2), or multiple (>2) peaks of PI(3)P association on phagosomes. (*G*) Statistical analysis of the duration of PI(3)P association on phagosomes containing uIgG particles (n = 26) and Moon particles (n = 39), and on macropinosomes containing uBSA particles (n = 33). Each data point is color-coded based on the number of PI(3)P peaks. Each boxplot indicates the interquartile range from 25% to 75% of the corresponding data set. The mean and median are demonstrated as the square and the horizontal line, respectively. Statistical significance is highlighted by p values (Kruskal-Wallis test with Dunn's test as a *post hoc* test for multiple-group comparisons) as follows: ****$p < 0.0001$, ns $p > 0.05$. Scale bars in all images, 5 μm.

engulfment during phagocytosis, the partial coating of ligands on Moon particles also affected the internalization process. In RAW 264.7 macrophages stably expressing actin-GFP, actin polymerized rapidly around particles during phagocytosis and then dissociated, which is expected for ligand-guided phagocytosis of uniform IgG particles (33). In contrast, actin was distributed predominantly near the IgG-coated side and later extended to the non-coated side during phagocytosis of the Moon particles (Fig. S6 *A*). We plotted actin intensity against time (Fig. S6 *B*), in which the actin intensity peak indicates the time when phagosome formation was completed (24). Overall, the relative intensity of actin, which was normalized to the cytosolic actin level, during phagocytosis of Moon particles was significantly less than that observed for uniform IgG particles (Fig. S6 *C*).

After the internalization of particles, the plasma membrane-derived phagosomes recruit a series of signaling molecules needed for maturation (9). To test whether the phagosome membrane remodeling is affected by the anisotropic presentation of ligands on particles they encapsulate, we examined the association of phosphatidylinositol 3-phosphate (PI(3)P) with phagosomes. PI(3)P is an early phagosome marker required for maturation and phagolysosome formation (34). It is either recruited through fusion with early endosomes (35) or synthesized *de novo* on phagosome membranes by phosphoinositide 3-kinase Vps34 (35,36). In RAW 264.7 macrophages transfected with 2×FYVE-GFP, which is a PI(3)P-binding sensor (37), phagosomes containing particles with various ligand presentations all displayed a homogeneous distribution of PI(3)P (Fig. S7 *A*). Phagosomes containing uniform IgG particles first exhibited an increase in 2×FYVE-GFP intensity, and then a decrease, resulting in a nearly symmetric peak in the intensity vs. time plot (Fig. 2 *B*). This indicates the transient association of PI(3)P on phagosomes. Most phagosomes containing uniform IgG particles exhibited a similar single 2×FYVE-GFP peak (Fig. 2 *F*). In contrast, a large fraction of phagosomes containing Moon particles and macropinosomes containing uniform BSA particles exhibited multiple peaks in 2×FYVE-GFP intensity (Fig. 2

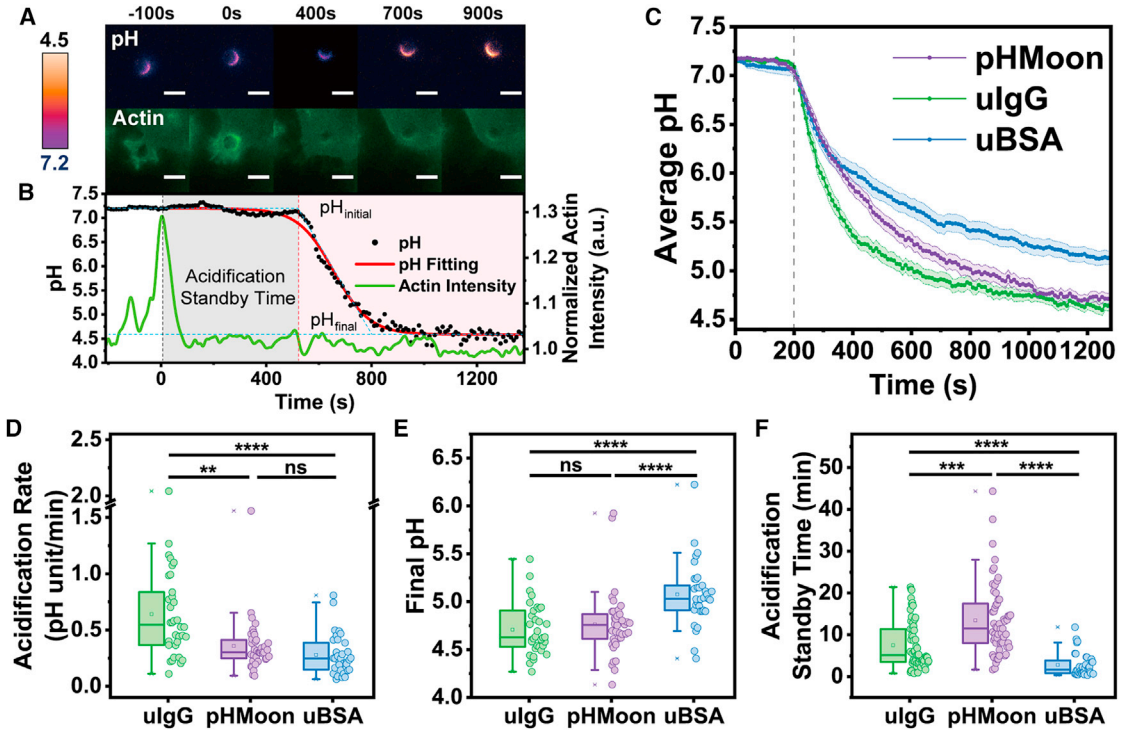

FIGURE 3 Phagosome acidification measurements using pHMoon Sensors. (*A* and *B*) Epifluorescences images (*A*) and line plots (*B*) showing changes of pH and normalized actin-GFP intensity of a representative phagosome containing a pHMoon sensor in an actin-GFP RAW 264.7 macrophage. The actin intensity was normalized to the cytosolic background level of actin. The time of internalization was identified as the actin peak and was arbitrarily set as time zero to align all plots. The gray shaded area highlights the acidification standby time. (*C*) The averaged pH-time plots of phagosomes containing different types of particle sensors as indicated: pHMoon (n = 38), uniform IgG (uIgG) (n = 34), and uniform BSA (uBSA) (n = 33). Error bar represents the standard error of the mean. To align all data plots, the acidification onset was arbitrarily set to 200 s. (*D* and *E*) Statistical analysis of acidification rate (*D*) and final pH (*E*) of single phagosomes encapsulating uIgG particles (n = 34), pHMoon particles (n = 38), and macropinosomes containing uBSA particles (n = 33). (*F*) Statistical analysis of acidification standby time of single phagosomes containing uIgG particles (n = 61), Moon particles (n = 59), and macropinosomes containing uBSA particles (n = 36). Each boxplot indicates the interquartile range from 25% to 75% of the corresponding data set. The mean and median are demonstrated as the square and the horizontal line, respectively. Statistical significance is highlighted by p values (Kruskal-Wallis test with Dunn's test as a *post hoc* test for multiple group comparisons) as follows: ****$p < 0.0001$, ***$p < 0.001$, **$p < 0.01$, ns $p > 0.05$. Scale bars in all images, 5 μm.

D and *E*), which indicates repeated association and dissociation of PI(3)P (Fig. 2 *B*). Additionally, the dissociation of 2×FYVE-GFP was slower, resulting in asymmetric peaks in the 2×FYVE-GFP intensity plots (Fig. 2 *C*). As a result of the slower dissociation and repeated association-dissociation of PI(3)P, phagosomes containing Moon particles were associated with PI(3)P for an overall prolonged duration than phagosomes containing uniform IgG particles (Figs. 2 *G* and S7 *B*). The PI(3)P association results demonstrate the striking differences in early phagosome remodeling between phagosomes containing Moon particles and ones containing uniform IgG particles.

Effect of particles with an anisotropic ligand presentation on phagosome acidification

Following transient association with PI(3)P, phagosomes acidify in their lumen. Acidification is a key step in the degradation of encapsulated pathogens and is driven by proton pump V-ATPases that are delivered by endosomes and lysosomes that fuse with maturing phagosomes (38). We examined how the asymmetric presentation of IgG on Moon particles affects this process. We used RAW 264.7 macrophages expressing actin-GFP so that we could quantify when acidification started relative to the completion of phagosome formation, which is indicated by a peak in actin intensity (24). The pHMoon particle sensors were imaged (in both pHrodo Red and CF640R channels) simultaneously with actin-GFP in cells after the particles were added to cells (Fig. 3 *A*). The measured fluorescence intensity ratio $I_{pHrodoRed}/I_{CF640R}$ was converted to pH based on the calibration plots. We observed that phagosomes acidified in three stages (Fig. 3 *B*). In the first stage, the phagosome lumen remained at a neutral pH of 7.2 for a few minutes after the completion of internalization, which was indicated by the intensity peak of actin-GFP. The period from time of phagosome completion (actin peak) to the time when rapid

acidification starts is referred as "acidification standby time." In the second stage phagosomes rapidly acidified from pH 7.2 to pH 5.0 within a few minutes, and then remained acidic at a final pH of 4.7 in the final stage. For quantification, the pH-time plots of single phagosomes were fitted with a sigmoidal-Boltzmann equation (28). The slope at the half response time is the acidification rate by definition. The acidification standby period of single phagosomes was then calculated as the time from the peak of actin-GFP intensity to the onset of rapid acidification (highlighted as the gray shaded area in Fig. 3 *B*). We found that the pHMoon-containing phagosomes acidified at an average rate of 0.36 ± 0.23 pH U/min and reached an average final pH of 4.8 ± 0.3. The average acidification standby time was 13.4 ± 8.5 min. By comparison, phagosomes containing uniform IgG particles acidified at an average rate of 0.64 ± 0.40 pH to a final pH of 4.7 ± 0.3, whereas phagosomes containing uniform BSA particles acidified at a rate of 0.28 ± 0.18 pH U/min to a final pH of 5.1 ± 0.3 (Fig. 3 *D* and *E*). Meanwhile, the pHMoon-containing phagosomes exhibited the longest acidification standby time (Fig 3 *F*). We found the delayed onset of acidification was correlated with the prolonged association of PI(3)P on pHMoon-containing phagosomes (Fig. S7 *C*–*E*).

Because pHMoon particles differ from uniform IgG particles in both the spatial presentation of ligands and the absolute amount of ligands, we next tested which one of these factors caused the differences in phagosome acidification. We systematically increased the total amount of IgG on uniform IgG particles by doubling and then quadrupling it. The different amounts of ligands were confirmed by noting the increase of intensity of fluorescently labeled IgG on particles. The acidification rate, final pH, and standby time of phagosomes containing uniform IgG particles with 1×, 2×, and 4× ligand density (Fig. S8 *A*) showed no statistical difference (Fig. S8 *B*–*D*). This result indicates that the amount of IgG on particles does not affect phagosome acidification. Therefore, we conclude that the asymmetric ligand presentation on pHMoon particles, rather than the amount of ligand present, was the cause of the changes in phagosome acidification, including both their delayed start and the slowdown of acidification kinetics. The surface anisotropy, however, exerted no effect on the final pH (Fig. 3 *C*).

Effect of particles with anisotropic ligand presentation on phagosomal proteolysis

Facilitated by acidification, phagosomal proteolysis is a key process in maturation in which engulfed pathogens are degraded by proteases such as cysteine cathepsins (39). To detect phagosomal proteolysis, we designed proteolysis-Moon Sensors which included a fluorgenic peptide $(CBZ\text{-}Phe\text{-}Arg)_2$-R110 (rhodamine 110, bis-(N-CBZ-L-phenylalanyl-L-arginine amide), dihydrochloride) on the particle surface. This rhodamine 110-based bis-peptide is non-fluorescent, but cleavage of one or both of the peptides by proteases results in a rhodamine 110 derivative that emits intense fluorescence (Fig. 4 *C*) (40). Specifically, proteolysis-Moon particles were conjugated with CF640R-SAv as the reference dye and then coated with the fluorogenic peptide by physical adsorption (Fig. 4 *A* and *B*). We calibrated the proteolytic response of the sensors in the presence of the protease trypsin *in vitro* (Fig. S9). The result shows that the proteolysis-Moon Sensors and uniform proteolysis sensors were coated with the same amount of peptides.

In RAW 264.7 macrophages stably transfected with actin-mCherry, we observed an intense increase in rhodamine 110 fluorescence from phagosomes within 20 min after completion of internalization. The time of internalization is indicated by the peak of actin intensity. The rhodamine 110 eventually reached a plateau (Fig. 3 *C* and *D*). The slope of the peptide fluorescence indicates the proteolytic capacity of phagosomes, and the plateau likely occurred when all the peptides on particles have been digested (41). As with the phagosome acidification plots, the fluorescence intensity of cleaved peptides from single phagosomes follows a sigmoidal-Boltzmann relationship with time. The slope at the half response time is the proteolysis rate. The time difference from internalization to the start of proteolysis is defined as the proteolysis standby time. Similar to the acidification standby results, phagosomes containing proteolysis-Moon particles had a delayed start of proteolysis (21.8 ± 7.0 min) compared with phagosomes containing uniform IgG particles (16.1 ± 6.8 min) (Fig. 4 *E*). However, they had a similar proteolysis rate, both of which were greater than that of the macropinosomes containing uniform BSA particles (Fig. 4 *F*). Previous studies have shown that proteases are more active in an acidic medium (42). Therefore, the delayed start of proteolysis in phagosomes containing the proteolysis-Moon particles is likely a consequence of delayed acidification. Results from the pH and proteolysis measurements altogether reveal two effects of anisotropic ligand presentation on phagosome maturation. It delays the onset of both acidification and proteolysis and slows down the kinetics of acidification. However, all this ultimately has no effect on the final pH or the proteolysis rate of phagosomes.

We further quantified the degradative capacities of phagosomes by labeling a few membrane markers: Ras-related protein Rab-7 (Rab7), lysosomal-associated membrane protein 1 (LAMP1), and microtubule-associated protein 1A/1B-light chain 3 (LC3). Rab7 is

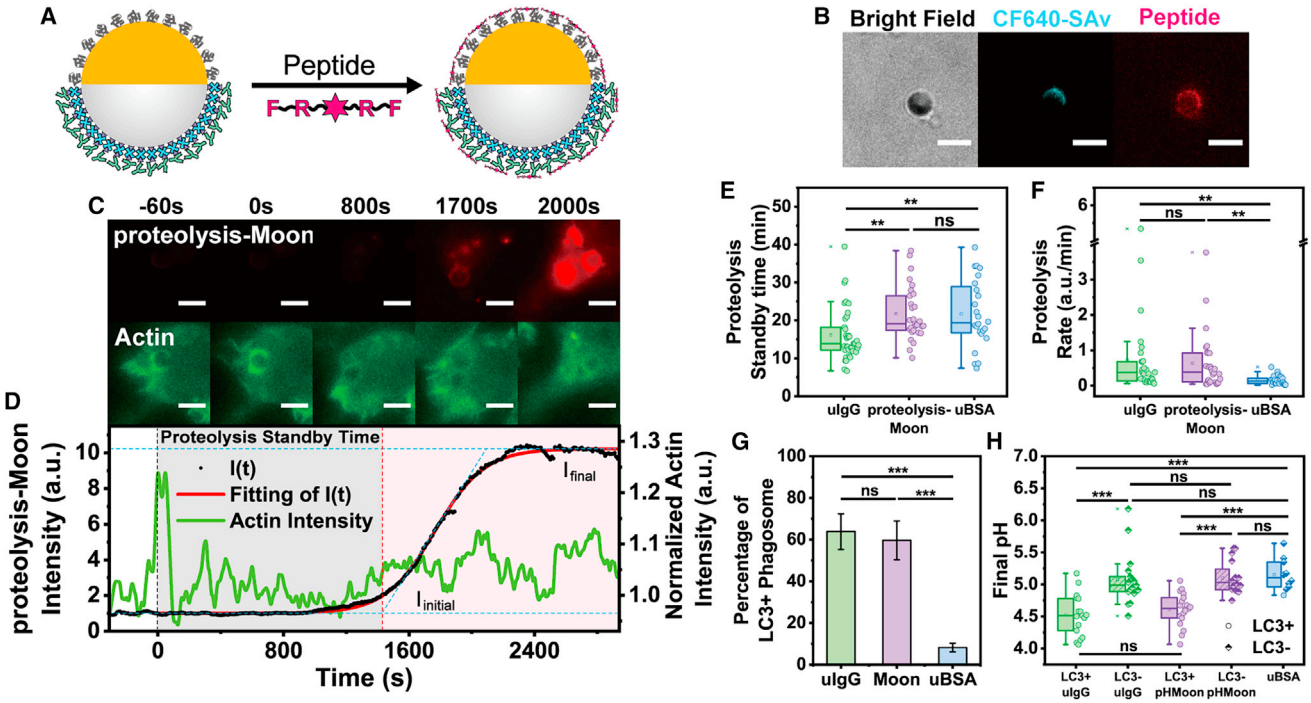

FIGURE 4 The degradative capability of phagosomes containing Moon particles. (*A*) Schematic illustration of the fabrication procedure of proteolysis-Moon particle sensors. (*B*) Bright-field and epifluorescence images of a proteolysis-Moon particle sensor. (*C* and *D*) Epifluorescence images (*C*) and line plots (*D*) showing intensity changes of a proteolysis-Moon particle sensor and actin-mCherry during phagosome maturation in a RAW 264.7 macrophage expressing actin-mCherry. The actin intensity was normalized to its cytosolic background level. The actin peak indicates the time of internalization and was arbitrarily set as time zero to align all line plots. The gray shade highlights the proteolysis standby time. (*E* and *F*) Statistical analysis of proteolysis standby time (*E*) and proteolysis rate (*F*) of single phagosomes containing proteolysis-Moon particles (n = 29) and uniform IgG (uIgG) particles (n = 30), and of macropinosomes containing uniuBSA particles (n = 25). (*G*) The percentage of LC3+ phagosomes containing uIgG particles (n = 427) and Moon particles (n = 446), and LC3+ macropinosomes containing uBSA particles (n = 384). Particles were incubated with cells for 40 min before imaging. (*H*) Statistical analysis of final pH of LC3+ phagosomes and LC3− phagosomes. LC3+ phagosomes containing uIgG particles (n = 17), LC3− phagosomes containing uIgG particles (n = 16), LC3+ phagosomes containing pHMoon particles (n = 19), LC3− phagosomes containing pHMoon particles (n = 16), macropinosomes containing uBSA particles (n = 10). Each boxplot indicates the interquartile range from 25% to 75% of the corresponding data set. The mean and median are demonstrated as the square and the horizontal line, respectively. Statistical significance is highlighted by p values (Kruskal-Wallis test with Dunn's test as a *post hoc* test for multiple-group comparisons) as follows: ***$p < 0.001$, **$p < 0.01$, ns $p > 0.05$. Scale bars in all images, 5 μm.

a marker for late phagosomes and LAMP1 is a phagolysosome marker (43). LC3 is not a prerequisite for phagosome maturation, but its presence marks phagosomes that acidify rapidly and degrade pathogens efficiently (44,45). We found that all three markers were distributed homogeneously over the phagosomes containing particles with different ligand presentations (Fig. S10 *A*–*C*). The percentage of marker positive phagosomes was similar for phagosomes containing Moon particles and phagosomes containing uniform IgG particles. By comparison, a much smaller fraction of macropinosomes containing uniform BSA particles were marked for Rab7, LAMP1, and LC3, indicating the lower degradative capacity (Figs. 4 *G*, S10 *D*, and *E*). Particularly, by separating the LC3+ and LC3− phagosomes, we found that the LC3+ phagosomes have lower final pH than LC3− phagosomes, which confirms the correlations between phagosome pH and degradation function (Figs. 4 *H* and S11). We have shown that the anisotropic ligand presentation on particles had no effect on either of the parameters.

Generality of findings in Dectin-1-mediated phagocytosis

To test the generality of our results from FcγR-mediated phagocytosis, we fabricated pHMoon particles coated with curdlan, a ligand for triggering Dectin-1-mediated phagocytosis (46,47). Dectin-1 is a pattern recognition receptor and like FcγRs, signals through tyrosine-based activation motif (48). To prepare curdlan-coated pHMoon particles, 3-μm silica particles were aminated and covalently conjugated with curdlan before the anisotropic coating of gold, but the remaining fabrication procedure was the same as for IgG-coated pHMoon particles (Fig. 5 *A*). Those particles also exhibited similar pH-dependent fluorescence emission (Fig. S12). Immunofluorescence images

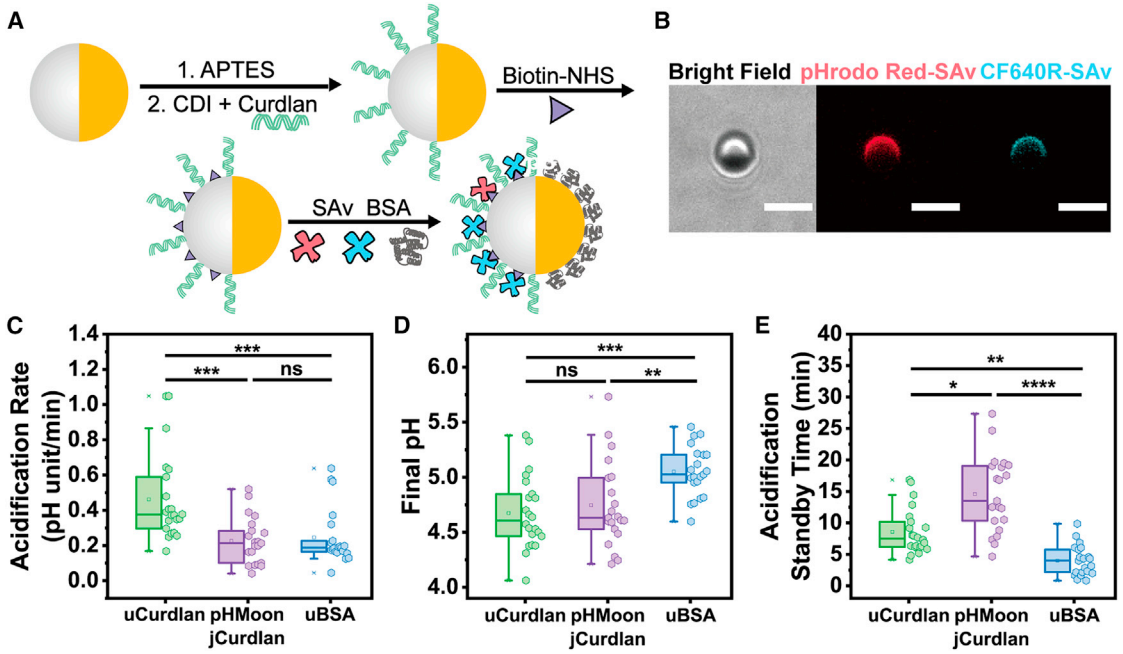

FIGURE 5 Dectin-1 receptor-mediated phagosome maturation measured by curdlan pHMoon Sensors. (*A*) Schematic illustration of the fabrication procedure of curdlan pHMoon Sensors. (*B*) Bright-field and epifluorescence images of curdlan pHMoon Sensors. (*C–E*) Statistical analysis of acidification rate (*C*), final pH (*D*), and acidification standby time (*E*) of single phagosomes encapsulating curdlan pHMoon particles (n = 21), uniform curdlan (uCurdlan) particles (n = 22), and macropinosomes containing uniform BSA (uBSA) particles (n = 21). Each boxplot indicates the interquartile range from 25% to 75% of the corresponding data set. The mean and median are demonstrated as the square and the horizontal line, respectively. Statistical significance is highlighted by p values (Kruskal-Wallis test with Dunn's test as a *post hoc* test for multiple group comparisons) as follows: ****$p < 0.0001$, ***$p < 0.001$, **$p < 0.01$, *$p < 0.05$, ns $p > 0.05$. Scale bars in all images, 5 μm.

reveal that the phagosome distribution of pSyk, which is a key signaling molecule downstream of Dectin-1 activation (48), follows the distribution of curdlan on particles (Fig. S13). The pHMoon-containing phagosomes acidified at a slower rate than those containing uniform curdlan particles (Fig. 5 *C*) and had the longest acidification standby time (Fig. 5 *E*). However, the anisotropic presentation of curdlan on particles had a negligible effect on the final pH of phagosomes (Fig. 5 *D*). These observations are strikingly similar to results from the FcγR-mediated phagosome maturation. Because FcγR and Dectin-1 represent different classes of innate immune receptors, this demonstrates the generality of our findings.

DISCUSSION

In this study, we investigated the effect of particles with an anisotropic ligand presentation on the degradative function of phagosomes. The key new technique used in this study is the Moon particle sensors that not only have anisotropic ligand presentation, but also enable the *in situ* imaging of acidification and proteolysis within single phagosomes. Using the Moon particles, we discovered that the anisotropic distribution of ligands differentially affects phagosome maturation and degradation. It delays the start of acidification and proteolysis in phagosomes, slows down the kinetics of acidification, and changes the membrane remodeling at the early stage of phagosome maturation. It, however, does not affect the final degradative capacity of phagosomes. The observations are general for phagocytosis mediated by either FcγR or Dectin-1 receptors, two representative classes of immune receptors in host-pathogen interactions. This finding demonstrates a mechanism by which the surface anisotropy of microbes impacts the progression of the degradation process within phagosomes during host-pathogen interactions.

There is increasing evidence demonstrating that bacteria and fungi have anisotropic surfaces (5,6). However, there is virtually nothing known about how such microbial surface anisotropy might impact microbial interactions with host immune cells. While studies using synthetic particles as model pathogens have extensively examined how the physiochemical properties of phagocytic cargos impact the phagocytosis process, almost all studies were focused on particles with uniform surface chemistry. In our previous study, we showed that an anisotropic coating of ligands on particles alters the mechanism of their internalization (21,22). Results from this study added new insights into the effects of particle surface anisotropy on phagosome maturation and degradation, which occur after

internalization. Together, the results broaden our view of the functional consequences of surface anisotropy on bacteria and fungi. Many bacteria have been found to alter their cell surface as a way to adapt to environmental changes. For example, it was suggested that *Escherichia coli* develops resistance to ampicillin by changing the morphology, biopolymer grafting density, and rigidity of its cell wall (49). *Pseudomonas aeruginosa* modulates the synthesis and structure of lipopolysaccharide on the outer membrane during chronic infections and in response to antibiotic treatments (50). While the particles used in our study do not fully represent bacteria, our results suggest that intracellular pathogens might use the anisotropic distribution of cell wall components to delay the onset of phagosome degradation as a possible strategy to prolong their survival and thus increase the probability of infection inside host immune cells. We expect that the Moon particle sensors will be useful tools for detailed investigation on the interplay between surface anisotropy and other physiologically relevant factors, such as receptor-ligand affinity, in host-pathogen interactions.

SUPPORTING MATERIAL

Supporting material can be found online at https://doi.org/10.1016/j.bpr.2021.100041.

AUTHOR CONTRIBUTIONS

M.J. and Y.Y. designed the research and wrote the manuscript. M.J. performed the experiments and analyzed the data. W.L. fabricated metal-coated particles. Y.-q.Y. provided MATLAB codes for particle fluorescence intensity analysis.

ACKNOWLEDGMENTS

We thank Glenn Walpole and Prof. Sergio Grinstein (University of Toronto, Canada) for providing plasmids. The fabrication and characterization of Janus particles were done at the Nanoscale Characterization Facility at Indiana University.

This work was supported by the National Institute of General Medical Sciences of the National Institutes of Health (NIH) under award number R35GM124918. Particle fabrication and experiments of actin dynamics in this work were supported by the National Science Foundation award CBET-1554078. The content is solely the responsibility of the authors and does not necessarily represent the official views of the NIH.

REFERENCES

1. Shapiro, L., H. H. McAdams, and R. Losick. 2002. Generating and exploiting polarity in bacteria. *Science.* 298:1942–1946.
2. Young, K. D. 2006. The selective value of bacterial shape. *Microbiol. Mol. Biol. Rev.* 70:660–703.
3. Dorobantu, L. S., S. Bhattacharjee, …, M. R. Gray. 2008. Atomic force microscopy measurement of heterogeneity in bacterial surface hydrophobicity. *Langmuir.* 24:4944–4951.
4. Loh, J. T., S. C. Ho, …, M. Schindler. 1993. Carbohydrate binding activities of Bradyrhizobium japonicum: unipolar localization of the lectin BJ38 on the bacterial cell surface. *Proc. Natl. Acad. Sci. U S A.* 90:3033–3037.
5. Beaussart, A., S. El-Kirat-Chatel, …, Y. F. Dufrêne. 2013. Single-cell force spectroscopy of probiotic bacteria. *Biophys. J.* 104:1886–1892.
6. Singh, M. K., and L. J. Kenney. 2021. Super-resolution imaging of bacterial pathogens and visualization of their secreted effectors. *FEMS Microbiol. Rev.* 45:1–12.
7. Virji, M. 2009. Pathogenic neisseriae: surface modulation, pathogenesis and infection control. *Nat. Rev. Microbiol.* 7:274–286.
8. Botelho, R. 2017. Phagocytosis and Phagosomes: Methods and Protocols, First edition. Humana.
9. Flannagan, R. S., V. Jaumouillé, and S. Grinstein. 2011. The cell biology of phagocytosis. *Annu. Rev. Pathol.* 7:61–98.
10. Dupré-Crochet, S., M. Erard, and O. Nüβe. 2013. ROS production in phagocytes: why, when, and where? *J. Leukoc. Biol.* 94:657–670.
11. Lukacs, G. L., O. D. Rotstein, and S. Grinstein. 1990. Phagosomal acidification is mediated by a vacuolar-type H+-ATPase in murine macrophages. *J. Biol. Chem.* 265:21099–21107.
12. Hoffmann, E., F. Kotsias, …, S. Amigorena. 2012. Autonomous phagosomal degradation and antigen presentation in dendritic cells. *Proc. Natl. Acad. Sci. U S A.* 109:14556–14561.
13. Doshi, N., and S. Mitragotri. 2010. Macrophages recognize size and shape of their targets. *PLoS One.* 5:1–6.
14. Champion, J. A., and S. Mitragotri. 2006. Role of target geometry in phagocytosis. *Proc. Natl. Acad. Sci. U S A.* 103:4930–4934.
15. Garapaty, A., and J. A. Champion. 2017. Tunable particles alter macrophage uptake based on combinatorial effects of physical properties. *Bioeng. Transl. Med.* 2:92–101.
16. Pacheco, P., D. White, and T. Sulchek. 2013. Effects of microparticle size and Fc density on macrophage phagocytosis. *PLoS One.* 8:1–9.
17. Zhang, Y., A. D. Hoppe, and J. A. Swanson. 2010. Coordination of Fc receptor signaling regulates cellular commitment to phagocytosis. *Proc. Natl. Acad. Sci. U S A.* 107:19332–19337.
18. Blander, J. M. 2004. Regulation of phagosome maturation by signals from toll-like receptors. *Science.* 304:1014–1018.
19. Bohdanowicz, M., G. Cosío, …, S. Grinstein. 2010. Class I and class III phosphoinositide 3-kinases are required for actin polymerization that propels phagosomes. *J. Cell Biol.* 191:999–1012.
20. Polando, R., U. G. Dixit, …, M. A. McDowell. 2013. The roles of complement receptor 3 and Fcγ receptors during Leishmania phagosome maturation. *J. Leukoc. Biol.* 93:921–932.
21. Gao, Y., and Y. Yu. 2013. How half-coated janus particles enter cells. *J. Am. Chem. Soc.* 135:19091–19094.
22. Sanchez, L., Y. Yi, and Y. Yu. 2017. Effect of partial PEGylation on particle uptake by macrophages. *Nanoscale.* 9:288–297.
23. Gao, Y., and Y. Yu. 2015. Macrophage uptake of janus particles depends upon janus balance. *Langmuir.* 31:2833–2838.
24. Scott, C. C., W. Dobson, …, S. Grinstein. 2005. Phosphatidylinositol-4, 5-bisphosphate hydrolysis directs actin remodeling during phagocytosis. *J. Cell Biol.* 169:139–149.
25. Yu, Y.-q., Z. Zhang, G. Walpole…, 2021. Transport motility of phagosomes on actin and microtubules regulates timing and kinetics of their maturation. *bioRxiv* https://doi.org/10.1101/2021.04.04.438376.
26. Naufer, A., V. E. B. Hipolito, …, M. R. Terebiznik. 2018. pH of endophagosomes controls association of their membranes with Vps34 and PtdIns(3)P levels. *J. Cell Biol.* 217:329–346.

27. Parthasarathy, R. 2012. Rapid, accurate particle tracking by calculation of radial symmetry centers. *Nat. Methods.* 9:724–726.

28. Shekhar, S., A. Cambi, …, J. S. Kanger. 2012. A method for spatially resolved local intracellular mechanochemical sensing and organelle manipulation. *Biophys. J.* 103:395–404.

29. Arppe, R., T. Näreoja, …, M. Schäferling. 2014. Photon upconversion sensitized nanoprobes for sensing and imaging of pH. *Nanoscale.* 6:6837–6843.

30. Gao, Y., S. M. Anthony, …, Y. Yu. 2018. Cargos rotate at microtubule intersections during intracellular trafficking. *Biophys. J.* 114:2900–2909.

31. Sánchez-Mejorada, G., and C. Rosales. 1998. Signal transduction by immunoglobulin Fc receptors. *J. Leukoc. Biol.* 63:521–533.

32. Swanson, J. A. 2008. Shaping cups into phagosomes and macropinosomes. *Nat. Rev. Mol. Cell Biol.* 9:639–649.

33. Freeman, S. A., J. Goyette, …, S. Grinstein. 2016. Integrins Form an expanding diffusional barrier that coordinates phagocytosis. *Cell.* 164:128–140.

34. Jeschke, A., N. Zehethofer, …, A. Haas. 2015. Phosphatidylinositol 4-phosphate and phosphatidylinositol 3-phosphate regulate phagolysosome biogenesis. *Proc. Natl. Acad. Sci. U S A.* 112:4636–4641.

35. Vieira, O. V., R. J. Botelho, …, S. Grinstein. 2001. Distinct roles of class I and class III phosphatidylinositol 3-kinases in phagosome formation and maturation. *J. Cell Biol.* 155:19–25.

36. Ellson, C. D., K. E. Anderson, …, P. T. Hawkins. 2001. Phosphatidylinositol 3-phosphate is generated in phagosomal membranes. *Curr. Biol.* 11:1631–1635.

37. Burd, C. G., and S. D. Emr. 1998. Phosphatidylinositol(3)-phosphate signaling mediated by specific binding to RING FYVE domains. *Mol. Cell.* 2:157–162.

38. Vieira, O. V., R. J. Botelho, and S. Grinstein. 2002. Phagosome maturation: aging gracefully. *Biochem. J.* 366:689–704.

39. Russell, D. G., B. C. Vanderven, …, R. S. Heyderman. 2009. The macrophage marches on its phagosome: dynamic assays of phagosome function. *Nat. Rev. Immunol.* 9:594–600.

40. Assfalg-Machleidta, I., G. Rotheb, …, W. Machleidt. 1992. Membrane permeable fluorogenic rhodamine substrates for selective determination of cathepsin L. *Biol. Chem. Hoppe Seyler.* 373:433–440.

41. Yates, R. M., and D. G. Russell. 2008. Real-time spectrofluorometric assays for the lumenal environment of the maturing phagosome. *Methods Mol. Biol.* 445:311–325.

42. Jancic, C., A. Savina, …, S. Amigorena. 2007. Rab27a regulates phagosomal pH and NADPH oxidase recruitment to dendritic cell phagosomes. *Nat. Cell Biol.* 9:367–378.

43. Kinchen, J. M., and K. S. Ravichandran. 2008. Phagosome maturation: going through the acid test. *Nat. Rev. Mol. Cell Biol.* 9:781–795.

44. Martinez, J., J. Almendinger, …, D. R. Green. 2011. Microtubule-associated protein 1 light chain 3 alpha (LC3)-associated phagocytosis is required for the efficient clearance of dead cells. *Proc. Natl. Acad. Sci. U S A.* 108:17396–17401.

45. Martinez, J., R. K. S. Malireddi, …, D. R. Green. 2015. Molecular characterization of LC3-associated phagocytosis reveals distinct roles for Rubicon, NOX2 and autophagy proteins. *Nat. Cell Biol.* 17:893–906.

46. Ferwerda, G., F. Meyer-Wentrup, …, G. J. Adema. 2008. Dectin-1 synergizes with TLR2 and TLR4 for cytokine production in human primary monocytes and macrophages. *Cell. Microbiol.* 10:2058–2066.

47. McIntosh, M., B. A. Stone, and V. A. Stanisich. 2005. Curdlan and other bacterial (1→3)-β-D-glucans. *Appl. Microbiol. Biotechnol.* 68:163–173.

48. Goodridge, H. S., C. N. Reyes, …, D. M. Underhill. 2011. Activation of the innate immune receptor Dectin-1 upon formation of a -Phagocytic synapse-^{TM}. *Nature.* 472:471–475.

49. Uzoechi, S. C., and N. I. Abu-Lail. 2020. Variations in the morphology, mechanics and adhesion of persister and resister E. Coli cells in reponses to ampicillin: AFM study. *Antibiotics.* 9:235.

50. Maldonado, R. F., I. Sá-Correia, and M. A. Valvano. 2016. Lipopolysaccharide modification in gram-negative bacteria during chronic infection. *FEMS Microbiol. Rev.* 40:480–493.